Journal Name

ARTICLE TYPE

Cite this: DOI: 10.1039/xxxxxxxxxx

Phase field modelling of spinodal decomposition in the oil/water/asphaltene system

Gyula I. Tóth*[a,b] and Bjørn Kvamme[b]

Received Date
Accepted Date

DOI: 10.1039/xxxxxxxxxx

www.rsc.org/journalname

In this paper the quantitative applicability of van der Sman / van der Graaf type Ginzburg-Landau theories of surfactant assisted phase separation [van der Sman *et al., Rheol. Acta*, 2006, **46**, 3] is studied for real systems displaying high surfactant concentrations at the liquid-liquid interface. The model is applied for the water/heptane/asphaltene system (a model of heavy crude oil), for which recent molecular dynamics (MD) simulations provide microscopic data needed to calibrate the theory. A list of general requirements is set up first, which is then followed by analytic calculations for the equilibrium properties of the system, such as the equilibrium liquid densities, the adsorption isotherm and the interfacial tension. Based on the results of these calculations, the model parameters are then determined numerically, yielding a reasonable reproduction of the MD density profiles. Results of time-dependent simulations addressing the dynamical behaviour of the system will also be presented. It will be shown, that the competition between the diffusion and hydrodynamic time scales can lead to the formation of an emulsion. We also address the main difficulties and limitations of the theory regarding quantitative modelling of surfactant assisted liquid phase separation.

1 Introduction

Surfactants are interface active agents, whose migration to the interface of two immiscible fluids can result in a formation of a mechanically stable mixture, i.e. an emulsion. Emulsions[1] play important role on many fields of our everyday life: They appear in pharmaceutical materials[2], cosmetics and even food processing[3], but also have significance in medical applications[4,5]. Besides these well-known fields of application, surfactants might become the future of crude oil recovery as well[6,7]: It has been discovered that alternating injection of water and CO_2 is a more efficient technique to recover the residual oil than traditional EOR (Enhanced Oil Recovery) methods based on exclusive water or CO_2 injection[8,9], proposing then the idea of utilizing a water/CO_2 emulsion instead. Although there are many surfactants producing water/CO_2 emulsions[10,11], we need specific materials capable of forming both water/CO_2 and water/oil emulsions. It seems that a special class of aspheltenes can be converted into such an emulsifier, which is capable of forming an oil/water emulsion in addition to the CO_2/water emulsion[12], thus offering a water CO_2/water $\rightarrow$ oil/water transition. If the transition was fast enough compared to the characteristic flow velocities used in conventional oil recovery, this technique could also solve CO_2 storage problems, thus becoming the basis of a new, environmentally sound EOR technique. Unfortunately, the microscopic physical processes behind the water/CO_2/asphaltene emulsion formation are not well understood[13], therefore, it is crucial to identify and study the basic mechanism(s) of emulsion formation in the framework of a multi-scale approach, ranging from atomistic (molecular dynamics) simulations to mesoscale (continuum) theories. Fortunately, molecular dynamics simulations provide data for the interfacial properties of the two-phase system on the microscopic level[14,15]. These data can be then used as input for continuum descriptions addressing mesoscale phenomena, which can be then verified by comparing the results to available experimental data[16].

Continuum theories describing a surfactant assisted liquid phase separation are based on the Ginzburg-Landau (GL) theory of first order phase transitions and originate from Gompper and Zschocke[17], and Theissen and Gompper[18]. Theissen and Gompper successfully addressed spontaneous emulsification, while the model of Teramoto and Yonezawa[19] has been used to describe droplet growth dynamics in the oil/water system. The most widespread version of the GL based models is developed by van der Sman and van der Graaf[20]. The model is based on the regularization of the surface Dirac-delta function of the sharp interface model of Diamant and Andelman[21]. A similar

[a] *Department of Physics and Technology, University of Bergen, Allégaten 55, 5007 Bergen, Norway. Tel: 47 5558 2742; E-mail: gyula.toth@ift.uib.no*
[b] *Institute for Solid State Physics and Optics, Wigner Research Centre for Physics, P.O.Box 49, 1525 Budapest, Hungary*

This journal is © The Royal Society of Chemistry [year]

approach was published by Teng, Chern and Lai[22]. Later Liu and Zhang[23] introduced a generalized model accounting also for the lateral interaction between adjacent surfactant layers. The new model has been successfully applied for describing the influence of the Marangoni effect generated by the inhomogeneous interfacial tension on droplet dynamics. A comparative study of the aforementioned models was published by Li and Kim[24], while Yun, Li and Kim[25] introduced a non-variational formalism of the dynamic equations. Despite the efforts, the models often suffer from physical inconsistency, such as the lack of surfactant-free solution and/or decreasing interface width with increasing surfactant amount at the interface. Furthermore, a numerical study of Engblom et al[26] gave strong evidences of that the partial differential equation has no solution under certain physically relevant circumstances. A detailed theoretical analysis of the generalized van der Sman / van der Graaf model and the demonstration of emulsion formation by numerical simulations has recently been done by Tóth and Kvamme[27] for systems featuring low surfactant amplitudes at the liquid-liquid interfaces. In contrast, atomistic simulations clearly show that in the heptane/water/asphaltene system, for example, the asphaltene mole fraction is close to 1 at the interface at equilibrium, together with vanishing surfactant concentration in the bulk liquids. Besides, in our previous study only pure diffusion dynamics has been used to demonstrate emulsion formation close a critical point, which is not satisfying in general.

The paper is structured as follows. In Section 2, we define a van der Sman / van der Graaf type free energy functional with the corresponding equilibrium (Euler-Lagrange) and dynamic equations. In Section 3, we set up a list of criteria the model parameters have to satisfy. In Section 4, a parameter fitting process will be presented for the heptane/water/asphaltene system, followed then by a study for the dynamic behaviour of the system. In Section 5 we summarize the results and draw the conclusions.

Table 1 Nomenclature. The lack of unit indicates dimensionless quantity.

symbol	unit	description
F	J	Helmholtz free energy
$\mathscr{F}$	J/m^3	free energy density
σ_0	J/m^2	interfacial tension (w/o surfactant)
δ_0	m	interface thickness (w/o surfactant)
w	J/m^3	free energy scale
ε_ϕ^2	J/m	Cahn-Hilliard gradient term coefficient
R	$J/(mol\,K)$	gas constant
T	K	temperature
v_m	m^3/mol	average molar volume
τ_ϕ	$kg/(m^3 s)$	liquid-liquid diffusion time scale
τ_ψ	$kg/(m^3 s)$	surfactant diffusion time scale
ρ	kg/m^3	mass density
$\mathbb{R}$	Pa	reversible stress tensor
$\mathbb{D}$	Pa	dissipative stress tensor
$\mathbb{A}$	Pa	Korteweg stress
μ	$Pa\,s$	viscosity
p	Pa	non-equilibrium thermodynamic pressure
D_0	m^2/s	liquid-liquid diffusion coefficient
D_ψ	m^2/s	surfactant diffusion coefficient
λ	m	length scale
ζ	m	fitted interface parameter
τ	s	time scale
β	-	inverse temperature
c	-	interaction coefficient between adjacent surfactant layers
a	-	surfactant exclusion strength
d	-	interface-surfactant coupling parameter
ϕ_0	-	equilibrium liquid density difference
ψ_0	-	eq. surfactant concentration in the bulk liquid
ψ_a	-	eq. surfactant concentration at the interface
ξ_0	-	relative interface width in equilibrium
$\tilde{\tau}_\psi$	-	relative surfactant diffusion time scale
$\tilde{w}$	-	Korteweg stress amplitude
$\tilde{\nu}$	-	viscosity
κ	-	relative interfacial tension
I	-	total amount of absorbed surfactant
q	-	amount of interfaces
γ	-	time scaling parameter
s	-	relative speed of phase separation

2 Model description

2.1 Free energy functional

The physical state of a binary fluid + surfactant system can be characterized by two, space and time continuous order parameters, the liquid-liquid order parameter $\phi(\mathbf{r},t)$ (which is proportional to the normalized mass density difference of the two liquids), and the (normalized) surfactant concentration, $\psi(\mathbf{r},t)$. The Helmholtz free energy of the inhomogeneous system is given in a functional form[17–20,22–24,27]:

$$F = \int dV \left\{ \mathscr{F}_{CH}(\phi) + \mathscr{F}_\psi(\psi) + \mathscr{F}_1(\phi,\psi) \right\} \quad . \tag{1}$$

Here $\mathscr{F}_{CH}[\phi(\mathbf{r},t)]$ stands for a traditional Cahn-Hilliard model of liquid-liquid phase separation:

$$\mathscr{F}_{CH}(\phi) = w\, g(\phi) + \frac{\varepsilon_\phi^2}{2}(\nabla\phi)^2 \quad , \tag{2}$$

where $g(\phi) = (1-\phi^2)^2/4$ is the usual double-well function, while the parameters w and ε_ϕ^2 can be related to microscopic quantities of the surfactant-free system (i.e. when $\psi \equiv 0$) as follows[27]:

$$w = (3/2)(\sigma_0/\delta_0) \qquad \text{and} \qquad \varepsilon_\phi^2 = (3/4)\sigma_0\,\delta_0 \quad , \tag{3}$$

where σ_0 is the equilibrium interfacial tension, and δ_0 the interface width defined by the equilibrium planar interface solution $\phi_0^*(x) = \tanh(x/\delta_0)$[27]. Furthermore, $\mathscr{F}_\psi$ is the free energy associated with the presence of the surfactant:

$$\mathscr{F}_\psi(\psi) = w\left\{ \frac{1}{\beta}[\psi\log\psi + (1-\psi)\log(1-\psi)] - \frac{c}{2}\psi^2 \right\} \quad , \tag{4}$$

where the logarithmic term is the simplest approximation of the entropy of mixing, while c accounts for the interaction between adjacent layers of the surfactant. The parameter β is associated with the inverse temperature as $w/\beta = (RT)/v_0$, where v_0 is the "effective" molar volume of the system (to be defined later), R the gas constant and T the temperature. Furthermore, $\mathscr{F}_1$ is a first

This journal is © The Royal Society of Chemistry [year]

order coupling between $\phi(\mathbf{r},t)$ and $\psi(\mathbf{r},t)$:

$$\mathscr{F}_1(\phi,\psi) = w\,\psi\left[-\delta_r(\phi)+\frac{a}{2}\phi^2\right] \ , \tag{5}$$

where $\delta_r(\phi)$ is the regularized surface-delta function introduced by Diamant and Andelman[21], while the second term is responsible for the exclusion of the surfactant in the bulk phases. We mention that there are different ways of regularizing the surface-delta function. It was introduced as $\delta_r(\phi) \propto (\nabla\phi)^2$ originally by van der Sman and van der Graaf[20], however, recent works indicate, that there are both general theoretical[27] and numerical[26] problems with this regularization. It has been revealed that the square-gradient coupling results in unphysical behaviour, namely, shrinking interface width and accelerating phase separation with increasing surfactant load[27], and, moreover, the dynamic equations have no stable solution under physically relevant circumstances[26]. In our recent work, we proposed a hybrid coupling $\delta_r(\phi) := \Lambda_1\, g(\phi) + \Lambda_2\,(\nabla\phi)^2$ yielding constant interface width, therefore making the entire surfactant load range accessible by numerical simulations[27]. Although our findings regarding the critical behaviour of the model are valid in general, this coupling also leads to unstable interfaces for high interface loads (i.e. when the surfactant concentration converges to 1 at the interface), which is again due to the presence of the square-gradient term[26]). Therefore, in the present work we choose "Model 3" of Engblom et al[26], proposing

$$\delta_r(\phi) := d\,g(\phi) \ , \tag{6}$$

leading to physically consistent behaviour, i.e. increasing interface width and decreasing interfacial tension and speed of phase separation as a function of the surfactant load[27] together with numerical stability of the dynamic equations[26].

Using the length scale $\lambda = \delta_0/2$ and the free energy density scale w results in the following dimensionless free energy functional:

$$\tilde{F} = \int d\tilde{V}\left\{\tilde{\mathscr{F}}_{CH}+\tilde{\mathscr{F}}_{\psi}+\tilde{\mathscr{F}}_1\right\} \ , \tag{7}$$

where $\tilde{F} = F/(w\lambda^3)$, and

$$\tilde{\mathscr{F}}_{CH} = g(\phi)+\left(\tilde{\nabla}\phi\right)^2 \tag{8}$$

$$\tilde{\mathscr{F}}_{\psi} = \frac{1}{\beta}\left[\psi\log\psi+(1-\psi)\log(1-\psi)\right]-\frac{c}{2}\psi^2 \tag{9}$$

$$\tilde{\mathscr{F}}_1 = \psi\left[-d\,g(\phi)+\frac{a}{2}\phi^2\right] \ . \tag{10}$$

The dimensionless planar interface solution of the surfactant-free system reads as

$$\phi_0^*(\tilde{x}) = \tanh(\tilde{x}/2) \ , \tag{11}$$

while the dimensionless interfacial tension becomes $\tilde{\sigma}_0 = 4/3$.

2.2 Equilibrium

When the two liquids are in thermodynamic equilibrium, the planar interface profile can be determined from the 1-dimensional Euler-Lagrange equations:

$$\frac{\delta\tilde{F}}{\delta\phi} = \frac{\partial\tilde{\mathscr{F}}}{\partial\phi}-\frac{\partial}{\partial\tilde{x}}\left[\frac{\partial\tilde{\mathscr{F}}}{\partial(\partial_{\tilde{x}}\phi)}\right]=0 \tag{12}$$

$$\frac{\delta\tilde{F}}{\delta\psi} = \frac{\partial\tilde{\mathscr{F}}}{\partial\psi}=\tilde{\mu}_{\psi} \ , \tag{13}$$

where $\delta\tilde{F}/\delta\chi$ denotes the functional derivative of $\tilde{F}=\int d\tilde{x}\{\tilde{\mathscr{F}}\}$ with respect to $\chi=\phi,\psi$, where $\tilde{\mathscr{F}} = \tilde{\mathscr{F}}_{CH}+\tilde{\mathscr{F}}_{\psi}+\tilde{\mathscr{F}}_1$, and

$$\tilde{\mu}_{\psi} = (\delta\tilde{F}/\delta\psi)_{\phi_0,\psi_0} \tag{14}$$

is the dimensionless diffusion potential corresponding to the homogeneous background state $(\pm\phi_0,\psi_0)$. (Note that this kind of potential cancels from the first equation, since $\tilde{\mathscr{F}}_{CH}$ and $\tilde{\mathscr{F}}_1$ are symmetric in ϕ[26].) The boundary conditions read as: $\phi^*(\tilde{x})_{\tilde{x}\to\pm\infty} = \pm\phi_0$ and $\psi^*(\tilde{x})_{\tilde{x}\to\pm\infty} = \psi_0$, where $\phi^*(\tilde{x})$ and $\psi^*(\tilde{x})$ represent a solution of the Euler-Lagrange equations [see Fig. 1(a)]. Note that the bulk surfactant load, ψ_0 is a free parameter of the theory. Using Eqns. (7)-(10), the Euler-Lagrange equations read as:

$$(1-d\,\psi)(\phi^3-\phi)+a\,\psi\,\phi = 2\,\partial_{\tilde{x}^2}\phi \tag{15}$$

$$\frac{1}{\beta}\log\frac{\psi(1-\psi_0)}{(1-\psi)\psi_0}-c(\psi-\psi_0)+\Delta f(\phi) = 0, \tag{16}$$

where $\Delta f = f(\phi)-f(\phi_0)$, whereas

$$f(\phi) = -d\,g(\phi)+\frac{a}{2}\phi^2 \ . \tag{17}$$

Applying $\tilde{x}\to\pm\infty$ in Eq. (15) results in the bulk equilibrium value

$$\phi_0^2 = \frac{1-(a+d)\psi_0}{1-d\,\psi_0} \tag{18}$$

of the liquid-liquid order parameter, as a function of the bulk surfactant concentration. Introducing $\hat{\phi}(\tilde{x}) := \phi(\tilde{x})/\phi_0$ then results in

$$\Delta f(\hat{\phi}) = \frac{\phi_0^2}{4}\left[2(a+d)(\hat{\phi}^2-1)-d\,\phi_0^2(\hat{\phi}^4-1)\right] \ . \tag{19}$$

2.3 Dynamic equations

The time evolution of the system is governed by the following convection-diffusion dynamics:

$$\tau_{\phi}\left[\partial_t\phi+\nabla\cdot(\phi\,\mathbf{v})\right] = \nabla^2\frac{\delta F}{\delta\phi} \tag{20}$$

$$\tau_{\psi}\left[\partial_t\psi+\nabla\cdot(\psi\,\mathbf{v})\right] = \nabla\cdot\left[\psi(1-\psi)\nabla\frac{\delta F}{\delta\psi}\right] \tag{21}$$

$$\rho\left[\partial_t\mathbf{v}+\nabla\cdot(\mathbf{v}\otimes\mathbf{v})\right] = \nabla\cdot(\mathbb{R}+\mathbb{D}) \tag{22}$$

$$\nabla\cdot\mathbf{v} = 0 \ , \tag{23}$$

where $\otimes$ denotes the dyadic product, while $\mathbb{R}$ and $\mathbb{D}$ are the reversible and dissipative stress tensors, respectively. The dissipative stress simply reads as

$$\mathbb{D} = \mu(\phi,\psi)\left[(\nabla\otimes\mathbf{v})+(\nabla\otimes\mathbf{v})^T\right] \ , \tag{24}$$

where $\mu(\phi,\psi)$ is the (density dependent) dynamic viscosity, while the non-classical reversible stress reads as[28,29]:

$$\mathbb{R} = -p\mathbb{I} + \mathbb{A} \ , \tag{25}$$

where p is the non-equilibrium thermodynamic pressure for the inhomogeneous system[18]:

$$-p = \mathscr{F} - \phi\frac{\delta F}{\delta\phi} - \psi\frac{\delta F}{\delta\psi} \ , \tag{26}$$

and $\mathbb{A}$ is a non-diagonal stress component, which can be determined via the condition of mechanical equilibrium, yielding[18,30–36]:

$$\nabla\cdot\mathbb{R} = -\phi\nabla\frac{\delta F}{\delta\phi} - \psi\nabla\frac{\delta F}{\delta\psi} \ . \tag{27}$$

Note that in equilibrium $\delta F/\delta\phi = 0$ and $\delta F/\delta\psi = \mu$ are constants, therefore, no flow is generated. Comparing Eqns. (25)-(27) then results in:

$$\mathbb{A} = -\nabla\phi\otimes\frac{\delta F}{\delta\nabla\phi} - \nabla\psi\otimes\frac{\delta F}{\delta\nabla\psi} \ . \tag{28}$$

2.3.1 Time scales

The relaxation times τ_ϕ and τ_ψ in Eqns. (20) and (21) can be related to diffusion coefficients as follows. For $\psi(\mathbf{t},t)\equiv 0$, Eq. (20) reads as $\partial_t\phi = D_\phi\nabla^2[(\phi^3-\phi)-(\kappa/w)\nabla^2\phi]$, where $D_\phi = w/\tau_\phi$. Applying $\phi = \pm 1+\delta\phi$, where $|\delta\phi|\ll 1$), yields the diffusion equation $\partial_t\delta\phi = D_0\nabla^2\delta\phi$ with $D_0 = 2D_\phi$. Similarly, Eq. (21) results in $\partial_t\psi = D_\psi\nabla^2\psi$ in the bulk phases (i.e. when $\phi\equiv\pm 1$) for $c\,\psi \ll \beta^{-1}\log[\psi/(1-\psi)]$, where $D_\psi = \beta^{-1}(w/\tau_\psi)$ is the surfactant diffusion constant. Scaling time by $\tau = \lambda^2(\tau_\phi/w) = \lambda^2/D_\phi = (\delta_0/2)^2(2/D_0)$ results in the dimensionless dynamic equations:

$$\partial_{\tilde{t}}\phi + \tilde{\nabla}\cdot(\phi\,\tilde{\mathbf{v}}) = \tilde{\nabla}^2\frac{\delta\tilde{F}}{\delta\phi} \tag{29}$$

$$\tilde{\tau}_\psi\left[\partial_{\tilde{t}}\psi + \tilde{\nabla}\cdot(\psi\,\tilde{\mathbf{v}})\right] = \tilde{\nabla}\cdot\left[\psi(1-\psi)\tilde{\nabla}\frac{\delta\tilde{F}}{\delta\psi}\right] \tag{30}$$

$$\partial_{\tilde{t}}\tilde{\mathbf{v}} + \tilde{\nabla}\cdot(\tilde{\mathbf{v}}\otimes\tilde{\mathbf{v}}) = \tilde{\nabla}\cdot(\tilde{\mathbb{R}}+\tilde{\mathbb{D}}) \tag{31}$$

$$\tilde{\nabla}\cdot\tilde{\mathbf{v}} = 0 \ . \tag{32}$$

Here the dimensionless dissipative and reversible stresses read as

$$\tilde{\mathbb{D}} = \tilde{\nu}[(\tilde{\nabla}\otimes\tilde{\mathbf{v}}) + (\tilde{\nabla}\otimes\tilde{\mathbf{v}})^T] \tag{33}$$

$$\tilde{\mathbb{R}} = \tilde{w}(-\tilde{p}\mathbb{I}+\tilde{\mathbb{A}}) \ , \tag{34}$$

respectively, where

$$-\tilde{p} = \tilde{\mathscr{F}} - \phi\frac{\delta\tilde{F}}{\delta\phi} - \psi\frac{\delta\tilde{F}}{\delta\psi} \tag{35}$$

$$\tilde{\mathbb{A}} = -\tilde{\nabla}\phi\otimes\frac{\delta\tilde{\mathscr{F}}}{\delta\tilde{\nabla}\phi} \tag{36}$$

(note that there is no gradient term for ψ in the free energy functional). The scales and the dimensionless model parameters are summarized in Table 2. For the sake of simplicity, we will not use

Table 2 Scales and dimensionless model parameters.

λ	τ	β^{-1}	$\tilde{\tau}_\psi$	$\tilde{w}$	$\tilde{\nu}$
$\frac{\delta_0}{2}$	$\frac{\delta_0^2}{2D_0}$	$\frac{2}{3}\frac{RT}{v_m}\frac{\delta_0}{\sigma_0}$	$\frac{\beta^{-1}}{2}\frac{D_0}{D_\psi}$	$\frac{3}{2}\frac{\sigma_0\delta_0}{D_0^2\rho}$	$\frac{\mu}{\rho}\frac{2}{D_0}$

˜ hereafter.

3 Analysis

3.1 General requirements

In our recent work[27] we presented calculations for the interfacial tension in case of small interface loads, where the interface load is defined as the maximum of the equilibrium surfactant field, i.e. $\psi_a = \psi^*(0)$ [see Fig 1(a)]. As we have shown, the model has a critical point at the critical surfactant load

$$\psi_c = \frac{1}{a+d} \ , \tag{37}$$

where the equilibrium planar surfactant profile becomes constant [$\psi^*(x)\equiv\psi_c$], while $\phi_0\equiv 0$ for $a\neq 0$, together with vanishing interfacial tension[27]. This means that we have a second-order phase transition at ψ_c. Since the surfactant concentration is homogeneous at the critical load, our previous results based on the assumption, that $(\psi_a-\psi_0)/\psi_0 \lesssim 1$ are valid in general for both $\psi_0/\psi_c\to 0$ (low surfactant loads) and $\psi_0/\psi_c\to 1$ (close to the critical point). In contrast, in real systems (such as an oil/water/asphaltene system), the interface load converges to 1 even at extreme low bulk surfactant loads [see Fig 2(b), for example], while the bulk equilibrium densities of the liquids do not change significantly, and the corresponding interfacial tension lowering is $\approx 30\%$[14]. In this case the constant surfactant approximation, together with the small amplitude assumption are invalid, and the problem must be re-analysed.

Summarizing, the general properties of the scenarios to be investigated are:

1. The bulk surfactant load is (extremely) low: $\psi_0 \ll 1$.
2. The interface load is high: $\psi_a \to 1$.
3. The equilibrium bulk liquid density variation is negligible: $\phi_0 \approx 1$.
4. The interfacial tension lowering can be significant: $|\sigma(\psi_0)-\sigma_0|/\sigma_0 \sim 1$.
5. The interface width remains finite.

The last condition is an extra condition emerging from the fact that the interface width diverges at the critical point in this model, which makes the critical point inaccessible by numerical simulations.

This journal is © The Royal Society of Chemistry [year]

3.2 Location of the critical point

Since high interface load is considered, it is reasonable to prescribe $\psi_c \geq 1$. The explanation is, that in this case the fully loaded interface occurs exclusively at $\psi_0 = 1$, while $\psi_a(\psi_0) < 1$ for $\psi_0 \in [0,1)$, i.e. the system cannot be overloaded [blue curve in Fig 1(b)]. In contrast, $\psi_c < 1$ would result in $\psi^*(x) \equiv \psi_c$ (an therefore $\psi_a = \psi_c$ as well) at $\psi_0 = \psi_c$, although $\psi_a > \psi_c$ is possible for $\psi_0 \in (0, \psi_c)$, i.e. the system could be overloaded [red curve in Fig 1(b)], which would be hard to interpret physically. Note, that $\psi_c \lesssim 1$ is theoretically acceptable, as long as the bulk surfactant load is extremely small (i.e. $\psi_0 \ll 1$), thus we never go close enough to the critical point to experience a decreasing $\psi_a(\psi_0)$.

3.3 Liquid-liquid equilibrium density

Now we analyse the value of ϕ_0 described by Eq. (18) for $\psi_0 \ll 1$, yielding

$$\phi_0 = 1 - \frac{a}{2}\psi_0 + O(\psi_0^2) \quad . \tag{38}$$

Therefore, $|\phi_0 - 1| < \varepsilon/2$ is satisfied for $\psi_0 < \varepsilon/a$, where ε is the acceptable order of magnitude of the variation in ϕ_0. Assuming that $a > 0$, $d > 0$ and $a + d \approx 1$ and $a \sim d$ (i.e. they are in the same order of magnitude), this condition is always true for

$$0 \leq \psi_0 \leq \varepsilon \quad . \tag{39}$$

Note that Eq. (38) shows the role of parameter a: with increasing a the critical point tends to 0, together with a decreasing ϕ_0. Since we want $\phi_0 \approx 1$, we may choose extremely small loads and/or a critical point $\psi_c \approx 1$.

3.4 Adsorption isotherm

As mentioned above, the interface load $\psi_a = \psi^*(0)$ is determined by Eq. (16), yielding the following implicit algebraic equation for ψ_a as a function of ψ_0:

$$\psi_a = \frac{\psi_0}{\psi_0 + (1-\psi_0)\exp\{\beta[\theta(\psi_0) - c(\psi_a - \psi_0)]\}} \quad , \tag{40}$$

where

$$\theta(\psi_0) = \frac{\phi_0^2}{4}\left[d(\phi_0^2 - 2) - 2a\right] \quad . \tag{41}$$

Here ϕ_0^2 is defined by Eq. (18) as a function of ψ_0. Eq. (41) is now analysed in case of $\psi_c \approx 1$ for 2 essentially different cases:

- $\psi_0 \to 0$: In this case, $\psi_a \to 0$ also applies, therefore, Eq. (41) can be expanded for $\psi_a \ll 1$, then solved for $\psi_a(\psi_0)$, yielding

$$\psi_a(\psi_0) = \exp(-\beta\,\theta_0)\,\psi_0 + O(\psi_0^2) \quad , \tag{42}$$

  where $\theta_0 = -(2a+d)/4$. Since $a > 0$ and $d > 0$, $\psi_a(\psi_0)/\psi_0 \geq 1$, i.e. we have adsorption.

- $\psi_0 \to \varepsilon$: For large interface loads, $\psi_a = 1 - \delta\psi_a$ can be written (where $0 < \delta\psi_a \ll 1$) at $\psi_0 = \varepsilon$. Using this in Eq. (40) together with $\delta\psi_a \leq \varepsilon^n$ yields then the condition

$$\beta \geq \frac{(n+1)\log(\varepsilon)}{\theta_0 - c} \quad , \tag{43}$$

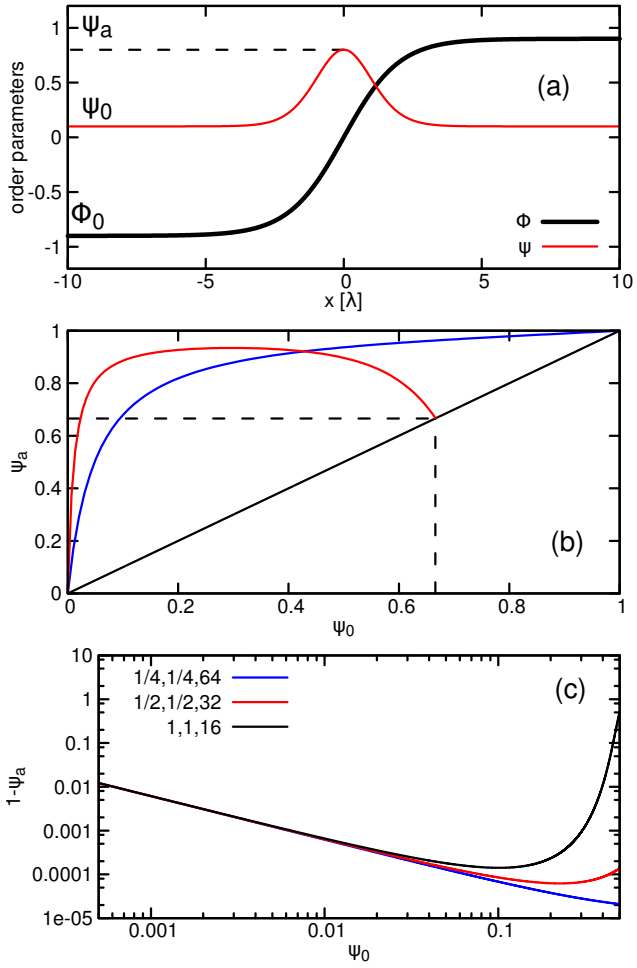

Fig. 1 (a) Schematic plot of an equilibrium interface. (b) Typical adsorption isotherms calculated from Eq. (40) in case of $c = 0$: (b) For $a = 1/4$, $d = 1/4$ and $\beta = 16$ the critical point is located at $\psi_c = 2$ (blue curve), prescribing normal adsorption isotherm at $\psi_0 \in [0,1]$. In contrast, $a = 3/4$, $d = 3/4$ and $\beta = 8$ (red curve) generates the critical point $\psi_c = 2/3$ and realizes a non-physical adsorption curve (the system can be overloaded, since $\psi_a > \psi_c$ is possible). (c) Adsorption curves in case of $a = 1/4$, $b = 1/4$ and $\beta = 64$ (blue), $a = 1/2$, $b = 1/2$ and $\beta = 32$ (red), and $a = 1$, $b = 1$ and $\beta = 16$ (black).

where we used the approximations $\Delta f(0) \approx \theta_0$ and $(1-\varepsilon)(1-\varepsilon^n) \approx 1$. Eq. (43) is a fairly simple condition for β as a function of the other model parameters a, d and c, which can be used to control the parameter fitting process.

Finally we note that we are relative free to choose the location of the critical point from the viewpoint of the adsorption isotherms, as indicated in Fig 1(c). Although ψ_c varies between $1/2$ and 2, the corresponding adsorption isotherms are almost identical for low bulk loads $\psi_0 < 0.01$. This is in accordance with the findings of Section 3.3.

3.5 Analysis of the Euler-Lagrange equations

Since the interface load converges to 1 for an extremely small bulk surfactant load $\psi_0 \ll 1$, one must consider the full Euler-Lagrange problem instead of the quasi-constant surfactant field

approximation applied in our recent work[27]. Using $\phi(x) = \phi_0\,\hat{\phi}(x)$ in Eq. (15), and re-scaling length as

$$\xi_0^2 = 1/[1-(a+d)\psi_0] \tag{44}$$

yields $\alpha_3(\psi)\hat{\phi}^3 - \alpha_1(\psi)\hat{\phi} = 2\,\partial_{\tilde{x}}^2\hat{\phi}$, where $x = \xi_0\tilde{x}$, $\alpha_3(\psi) = \frac{1-d\,\psi}{1-d\,\psi_0}$, and $\alpha_1(\psi) = \frac{1-(a+d)\psi}{1-(a+d)\psi_0}$. Approximating the coefficients *temporarily* as constants yields

$$\hat{\phi}(\tilde{x}) \approx \sqrt{\alpha_1/\alpha_3}\,\tanh[\sqrt{\alpha_1}(\tilde{x}/2)]\ , \tag{45}$$

which results in $\hat{\phi}(\tilde{x}) = \tanh(\tilde{x}/2)$ for $\tilde{x} \to \pm\infty$, but prescribes

$$\hat{\phi}(\tilde{x}) = \frac{\alpha_1^0}{\sqrt{\alpha_3^0}}\left(\frac{\tilde{x}}{2}\right) + O(\tilde{x}^3) \tag{46}$$

around $\tilde{x} = 0$, where $\alpha_1^0 = \frac{1-(a+d)\psi_a(\psi_0)}{1-(a+d)\psi_0}$ and $\alpha_3^0 = \frac{1-d\,\psi_a(\psi_0)}{1-d\,\psi_0}$. As one can see, the slope $(\alpha_1^0/\sqrt{\alpha_3^0})$ becomes 0 at $\psi_0 = 1/d$ and at $\psi_a(\psi_0) = \psi_c$, thus generating $\hat{\phi}^*(\tilde{x}) = 0$ and $\psi^*(\tilde{x}) = const$ around $\tilde{x} = 0$. Nevertheless, the first case is not relevant *at all*, since $\psi_0 = 1/d > \psi_c = 1/(a+d)$ always applies for $a > 0$ and $d > 0$. The second case, however still in the scope in case of $\psi_c < 1$, if the surface can be overloaded. Although it may happen at an extremely small bulk surfactant load, Eq. (40) suggest that it is the only value of ψ_0 at which this kind of solution exists. Although we did not experienced any difficulty in our calculations from this source, this finding further supports the condition $\psi_c \gtrsim 1$.

Having the 1 dimensional solution of the Euler-Lagrange equations $\phi^*(x)$ and $\psi^*(x)$, the interfacial tension can be measured as the function of the bulk surfactant load ψ_0[27]:

$$\sigma(\psi_0) = \int dx\{\mathscr{F}[\phi^*(x),\psi^*(x)] - \mathscr{F}_0 - \mu[\psi^*(x)-\psi_0]\}\ , \tag{47}$$

where $\mathscr{F}_0 = \mathscr{F}[\phi_0,\psi_0]$. The relative interfacial tension is defined as $\kappa(\psi_0) = \sigma(\psi_0)/\sigma_0$ while the relative interfacial tension drop reads as $\Delta\kappa := 1-\kappa(\psi_0)$. We mention, that in this work ψ_0 is not a relevant parameter, since we have only the condition $\psi_0 \ll 1$. Instead, it is worth to express κ as a function of the total amount of the absorbed surfactant, which is defined as

$$I(\psi_0) := \int_{-\infty}^{+\infty} dx\{\psi^*(x) - \psi_0\}\ . \tag{48}$$

For highly loaded interfaces, the approximations for the profiles used in our previous work fail, therefore, numerical solution of the Euler-Lagrange equation is needed, from which $\kappa(\psi_0)$ and $I(\psi_0)$ can de determined also numerically, resulting in a numerical $\kappa(I)$ relationship.

4 The oil/water/asphaltene system

4.1 Calibration of the model

Figure 2 shows equilibrium profiles in the the heptane/water/asphaltene system evaluated from recent molecular dynamics (MD) simulations[14]. Panel c displays a highly loaded interface, for which all our criteria apply. Note, that mass densities of the materials are shown, which have to be transformed into $\phi^*(\tilde{x})$ and $\psi^*(\tilde{x})$. The mass density is a conservative quantity, therefore, ϕ is also conservative, since they are related to each other via

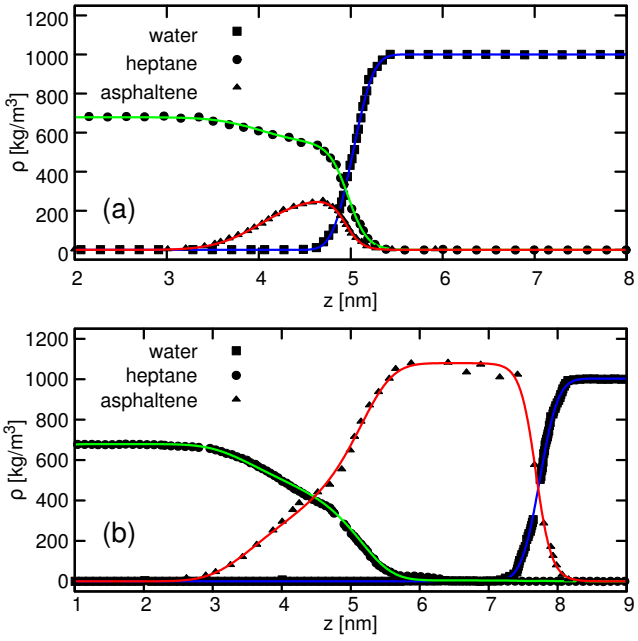

Fig. 2 Equilibrium profiles in the heptane/water/asphaltene system from molecular dynamics simulations (symbols)[14], and the analytical fits (solid curves) using linear combination of different hyperbolic tangent functions.

$$\phi^*(x) = \frac{\rho_w(x)}{\rho_w^0} - \frac{\rho_h(x)}{\rho_h^0}\ , \tag{49}$$

where the equilibrium mass density profiles of the water and heptane, $\rho_w(x)$ and $\rho_h(x)$, are normalized by their maxima, ρ_w^0 and ρ_h^0, respectively. This generates the conservative quantity $\phi \in [-1:1]$. Similarly, ψ can be simply interpreted as $\psi^*(x) := \rho_a(x)/\rho_a^0 \in [0,1]$. The parameters can be fitted by using the (almost) surfactant-free [see Fig. 2(a)] and the highly loaded [see Fig. 2(b)] cases as follows. Assuming that the water/heptane interface width is not affected significantly at small surfactant loads (this will be discussed later), the equilibrium liquid-liquid profile is approximated as $\phi(z) \approx \tanh[z/\zeta]$, yielding the derivative $(d\phi/dz)|_{z=0} = 1/\zeta$. ζ can be then fitted by using the MD profiles shown in Fig. 2(a), yielding $\zeta = 0.25743$ nm. The (dimensionless) total amount of the adsorbed surfactant is defined as:

$$I := \int_{-\infty}^{+\infty} dx\{\psi(x) - \psi_0\}\ , \tag{50}$$

where we use the dimensionless length $x := z/(\zeta/2)$. In case of $\psi_0 \to 0$ Eq. (55) is equivalent to $\int_{-\infty}^{+\infty} dx\{\psi(x)\}$, which can be measured on the highly loaded interface shown in Fig. 3(b), yielding $I_0 = 24$. Furthermore, the corresponding interfacial tension lowering emerging from the MD simulations is $\Delta\kappa \approx 0.3$. Instead of this, however, we choose $\kappa_0 = 0.35$ (half of the simulation result) for the following reasons:

This journal is © The Royal Society of Chemistry [year]

- Although experimental values are found to be less than $\Delta\kappa = 0.3$ in real crude oil/water/asphaltene systems[37], we would like to give clear evidence that emulsion formation in these system is not primarily interfacial tension driven.

- The physical parameters vary from sample to sample in real systems. In order to demonstrate the essence of the emulsion formation process in a general, theoretical oil/water/asphaltene system, we only need the correct order of magnitude of the different physical quantities.

The model parameters now have to be fitted for fixed I_0 and κ_0, and $\psi_0 \to 0$ and $\psi_a \to 1$, so that the equilibrium profiles $\phi^*(x)$ and $\psi^*(x)$ give reasonable fit to the MD results.

In our model there are 4 parameters, namely, a, d, β and c. Note, however, that not all these parameters are equally important. Basically 2 groups of them can be defined. The first contains a and d, and the second β and c, respectively, based on the role played on the level of the free energy functional. a and d are coupling parameters between ϕ and ψ, yielding a shift in ϕ_0 in the Cahn-Hilliard model (as discussed before). Since (i) the location of the critical point is a function of $a+d$, (ii) ϕ_0 is a function of a in the $\psi_0 \to 0$ limit, and (iii) the zero derivative condition at ϕ_0 depends on d (showing that they play only a slightly different individual role), we will work with $a = d$. The relationship between β and c is also similar, since they account for energy contributions associated with (exclusively) ψ. Since it has recently been shown that the logarithmic term must present in order to have physical adsorption isotherms[27], c is considered only as a modifying term, and without further thermodynamic informations we choose $c = 0$.

The parameter fitting process is the following. The 1-dimensional Euler-Lagrange equations are solved numerically for a given parameter set $a = d, \beta$ and ψ_0 first, then we measure I and κ, together with comparing the equilibrium profiles to the MD results. Since the target values I_0 and κ_0 are defined, this is an iterative process for ψ_0. Alternatively, one also can solve the 1-dimensional dynamic equations instead of the Euler-Lagrange equations, where the total amount of ψ is fixed. Since in case of $\psi_0 \to 0$ $\int_{-\infty}^{+\infty} dx\{\psi(x,t)\}$ coincides with I defined by Eq. (55), it is convenient to use the dynamic equations with the initial conditions $\phi(x,0) = \tanh(x/2)$ and $\psi(x,0) = I_0/L$, where L is the length of the simulation box. The system converges to equilibrium, i.e. a solution of the Euler-Lagrange equations. Therefore, all necessary quantities (the bulk surfactant load, the interface load, the relative interfacial tension, and the total absorbed amount) can be measured as a function of β. Since at constant $a = d$ the surface load ψ_a converges to 1 as $\beta \to \infty$ [see Eq. (40)], for a conservative dynamics ψ_0 must converge to 0 and I to I_0 as well. Therefore, we calculate ψ_0, ψ_a, R and κ as a function of β at constant $a = d$. This process is convenient in the sense that, due to the conservative dynamics, one of the required target values is "fixed". The results are shown in Fig 3. According to panel (b), the relative interfacial tension shows a non-trivial behaviour as a function of β, and seems to converge for $\beta \to \infty$, together with $\psi_0 \to 0$, $\psi_a \to 1$ and $R = I \to I_0$. Calculating then $\kappa(\beta)$ as a function of $a = d$ shows increasing tendency with increasing $a = d$ for $\beta > 16$ [see panel (c)], thus indicating $\psi_c < 1$. At $a = d = 0.575$ the critical point reads as $\psi_c \approx 0.87$, while $\psi_0 = 2.37 \times 10^{-4}$, $\psi_a = 1 - 10^{-5}$ and $R = 2 \times 10^{-4}$ at $\beta = 46$, showing that all the conditions are practically satisfied. Further increasing $a = d$ generates $\kappa = 0.35$ at lower β. For example, $a = d = 0.6$ generates $\psi_c = 0.83$, and $\kappa = 0.35$ occurs at $\beta = 25$, however, $\phi_0 = 1.2 \times 10^{-2}$ and $\psi_a = 0.98$, showing that one should search for the lowest possible $a = d$ at which $\kappa = 0.35$ can be realized for a finite β, together with vanishing ψ_0, and $\psi_a \approx 1$ and $\phi_0 \approx 1$. As shown in panel (d), the equilibrium $\psi^*(x)$ profile for $a = d = 0.5875$, $\beta = 32$ and $\psi_0 \approx 2.3 \times 10^{-3}$ is an acceptable agreement with the MD results.

One should not forget that the surfactant-free interface thickness (ζ) was estimated by using the profiles shown in Fig. 2.a, thus resulting in a slightly overestimation. The rate can be determined via calculating the numerical solution for I measured from Fig. 2.a, resulting in $\approx 1.05\zeta$ as the real interface width. Note that only I depends on ζ, but not κ and, moreover, $\kappa(I)$ saturates as a function of I, resulting in a quasi-constant behaviour at the fitting point $I_0 = 24$, therefore, a 5% shift in I_0 results in negligible difference in κ (see Fig. 4.b, for example). Therefore, the parameter fitting process doesn't have to be repeated with a corrected ζ. Nevertheless, we shall choose the length scale $\lambda = (\zeta/1.05)/2 \approx 0.12$ nm.

The only free parameter of the parameter fitting process is the bulk surfactant load, ψ_0. The source of this uncertainty is that the only condition ψ_0 reads as $\psi_0 \ll 1$. Nevertheless, it is worth to investigate how the results depend on ψ_0. We have two quantities fixed, namely, the total absorbed amount, I_0, and the relative interfacial tension, κ_0. The question is how the parameters β and $a = d$ change as a function of ψ_0, while keeping $I = I_0$ and $\kappa = \kappa_0$ unchanged. Assuming that ψ_0 changes as $\psi_0 \to (1+s)\psi_0$, where $s \ll 1$, and the parameters change as $a \to (1+h_1)a$, $d \to (1+h_1)d$, and $\beta \to (1+h_2)\beta$, the change in the interfacial tension and the interface load reads as:

$$d\kappa = \frac{\partial\kappa}{\partial s}s + \frac{\partial\kappa}{\partial h_1}h_1 + \frac{\partial\kappa}{\partial h_2}h_2 = 0 \ ; \qquad (51)$$

$$dI = \frac{\partial I}{\partial s}s + \frac{\partial I}{\partial h_1}h_1 + \frac{\partial I}{\partial h_2}h_2 = 0 \ , \qquad (52)$$

respectively. The derivatives in the equations above have to be measured numerically for a given β, $a = d$ and ψ_0. The solution h_1 and h_2 can be then determined as a function of s, therefore, the derivatives $\partial a/\partial\psi_0 = (a/\psi_0)(h_1/s)$, $\partial d/\partial\psi_0 = (d\psi_0)(h_1/s)$ and $\partial\beta/\partial\psi_0 = (\beta/\psi_0)(h_2/s)$ can be calculated, showing how $a = d$ and β should change as a function of ψ_0, together with preserving I and κ. Fig 4(a) shows the order parameter profiles at the fitting point, namely, $I = 24$ and $\kappa = 0.35$ in case of $\beta = 16$ (blue), $\beta = 32$ (black) and $\beta = 42$ (red). The corresponding bulk surfactant loads read as $\psi_0 = 2.3 \times 10^{-2}$, 2.3×10^{-3} and 4.1×10^{-4}, respectively, indicating a range of 2 orders of magnitude, while

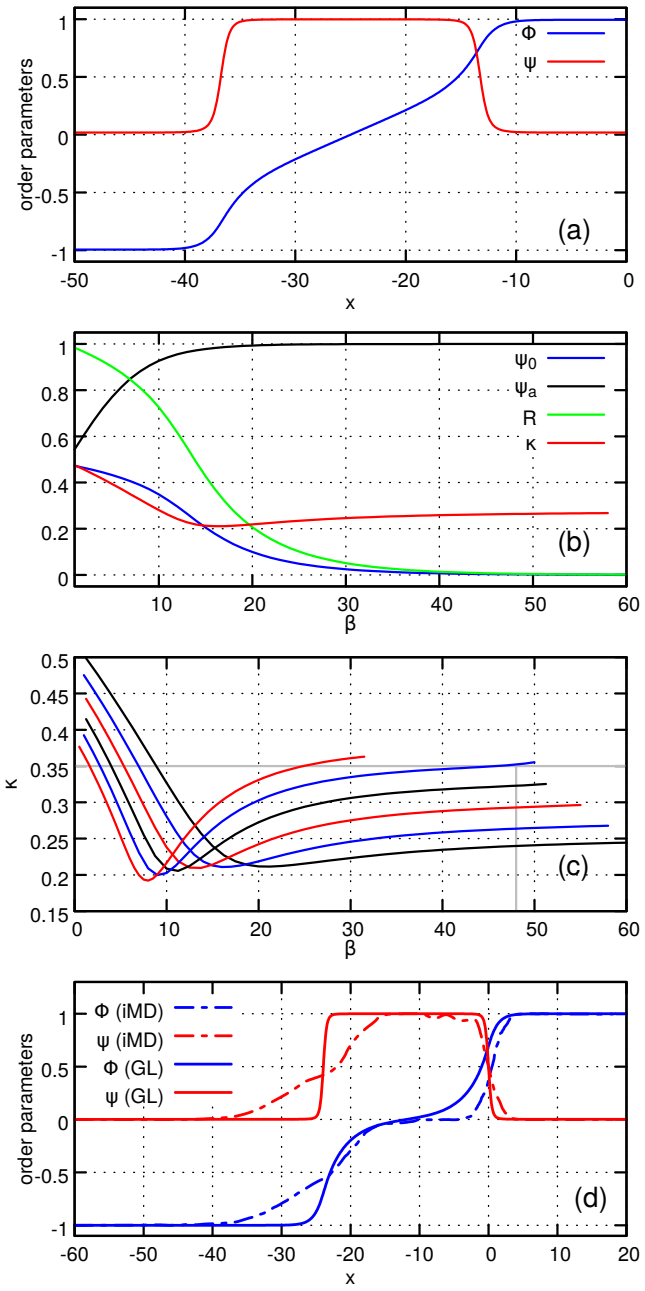

Fig. 3 Calibration process. (a) Converged (equilibrium) solution for $I_0 = 24$, $c = 0$, $a = d = 1/2$ at $\beta = 32$. (b) bulk surfactant load (ψ_0), surface load (ψ_a), remnant amount [$R = (I_0 - I)/I_0$], and relative interfacial tension (κ) as a function of β at $c = 0$, $a = d = 1/2$. (c) Relative interfacial tension as a function of β in case of $I_0 = 24$, for $a = d = 0.475, 0.5, 0.525, 0.55, 0.575$ and 0.6 (from bottom to top at $\beta = 30$, respectively). (d) Equilibrium order parameter profiles from molecular dynamics simulations (dashed) and from the present model (solid) for $I_0 \approx I = 24$, $\beta = 32$, $a = d = 0.5875$. The bulk load read as $\psi_0 = 2.3 \times 10^{-3}$.

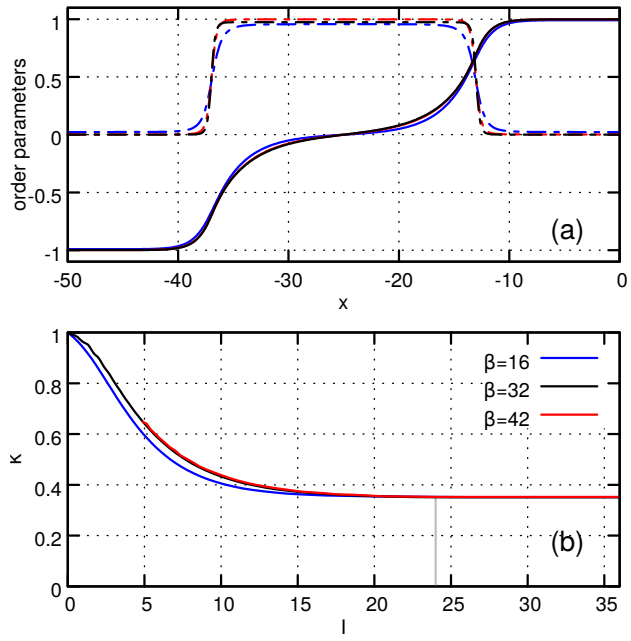

Fig. 4 Dependence of the parameter fitting process on the value of the bulk surfactant load, ψ_0. (a) Equilibrium profiles fitted to MD results in case of $\psi_0 = 2.3 \times 10^{-}2, 2.3 \times 10^{-3}$, and 4.1×10^{-4}. Note the increasing interface width in $\psi^*(x)$ with increasing ψ_0. (b) Relative interfacial tension vs total absorbed amount I for $\beta = 16, 32$ and 42. The gray vertical line indicates the point of parameter fitting $I_0 = 24$. The corresponding bulk loads read as $\psi_0 = 2.3 \times 2.3 \times 10^{-2}, 2.3 \times 10^{-3}$ and 4.1×10^{-4}, respectively.

$a = d$ do not change significantly. Comparing Figs 3(d) and 4(a), it is obvious that smaller β generates smaller slope for the surfactant profile at the interface, offering a better fit to the MD results in this regime. Contrary to this, ψ becomes significant in the bulk, which, however, may be numerically wieldier, does not reflect reality. A more interesting behaviour can be observed by investigating the relative interfacial tension (κ) as a function of the total interface load (I). Fig 4(b) shows that, regardless of the value of β, κ converges to the prescribed value $\kappa = 0.35$ as a function of I. This means that the interfacial tension cannot be reduced by loading the interface further. This behaviour is absolutely in agreement with experimental results[37]. The physical reason of this phenomenon is the following. At a critical total interface load, the asphaltene layer becomes wide enough to entirely separate the water and the heptane. At this stage, two interfaces emerge from the highly loaded water/heptane interface: a water/asphaltene and an asphaltene/heptane interface, with bulk asphaltene in between. Since the bulk asphaltene has no contribution to the interfacial energy, adding more asphaltene to the system cannot reduce he interfacial tension further. This characteristic behaviour is also present in the Ginzburg-Landau formalism, however, we have to mention, that we do not have two separated interfaces, because of the physical interpretation of the order parameters: ϕ is interpreted as a *difference* of the (normalized) densities of the water and the heptane, we cannot describe the bulk surfactant, i.e. when none of the two liquids are present. In other words, there are only 2 independent variables. In contrast, in order to describe 3 independent interfaces between 3 phases, 3 independent order parameters are needed. This necessitates further development and an another formulation of the model, which is also supported by additional findings discussed later.

This journal is © The Royal Society of Chemistry [year]

4.2 Spinodal descomposition

After fitting the model parameters to MD results, we study the dynamic behaviour of the system. As a reference, first we solve the kinetic equations *without* fluid flow (i.e. $\tilde{w}=0$ is considered in the Navier-Stokes equation), then the fluid flow will be 'switched on'. In case of small hydrodynamic force, i.e. $\tilde{w} \propto (\sigma_0 \delta_0)/(D_0^2 \rho) \ll 1$, one can expect negligible flow field generation compared to the diffusion. In contrast, in case of $\tilde{w} \approx \tilde{\nu} \gg 1$, the phase separation process is essentially hydrodynamics driven, and may accelerate even with orders of magnitude compared to the diffusion-driven case. Nevertheless, for large viscosities ($\tilde{\nu} \gg \tilde{w}$) the fluid flow is suppressed, therefore, the transport processes are governed by the diffusion dynamics again. One can see that there are many possibilities, and the dynamical behaviour of the system depends on the competition between the diffusion and hydrodynamic time scales. Indeed, the viscosity of the asphaltene/heptane system, for example, strongly depends on the asphaltene content (it changes several orders of magnitude)[38]. This means that it might happen that asphaltene migration to the water/heptane interfaces practically stops the hydrodynamics driven (fast) phase separation. Since the net transport of water and heptane is possible only via diffusion through the asphaltene layer, the phase separation becomes diffusion controlled. This can stabilize the emulsion, since the phase separation practically stops on the hydrodynamic time scale.

4.2.1 Dynamic parameters

The parameters of the theory, as indicated by Table 1, can be associated with simple physical quantities, such as the interfacial free energy, interface thickness, density, temperature, molar volume, diffusion coefficient and viscosity. A large amount of data are available for the water/heptane/asphaltene system in the literature. At reservoir circumstances (room temperature, $T \approx 300K$, and $10-100$ MPa pressure) the bulk mass densities read as $\rho_w = 1000$ kg/m^3, $\rho_h = 700$ kg/m^3 and $\rho_a = 1050$ kg/m^3 for the water, heptane, and asphaltene, respectively[14], yielding the average $\rho = 850$ kg/m^3. The length scale reads as $\lambda = 0.12$ nm, while the interfacial tension of the surfactant-free system is $\sigma_0 = 40$ mJ/m^2[14]. These, together with our choice $\beta = 32$ yield the average molar volume of the system $v_0 = (2/3)(RT)(\delta_0/\sigma_0)\beta \approx 160$ cm^3/mol, which almost perfectly matches with the molar volume of the heptane $v_h = 140$ cm^3/mol, thus showing the self-consistency of the parameter fitting process for β: although β has been fitted on a seemingly entirely different basis, it consistently recovers the molar volume of a highly dilute heptane/asphaltene system, a scenario which was actually considered during the fitting process. The diffusion constant for the heptane in water is in the order of $D_0 = 7.0 \times 10^{-10}$ m^2/s[39], while the typical diffusion constant of the asphaltene in heptane reads as $D_\psi = 1.5 \times 10^{-10}$ m^2/s[40]. The kinematic viscosities read as $\mu_w^0 = 1$ mPas[41] and $\mu_h^0 = 0.4$ mPas[38] for the pure water and heptane, respectively. The viscosity of the heptane/asphaltene system reads as[38]

$$\mu_h(\psi)/\mu_h(0) = 1 + A\left[\exp(b\,\psi) - 1\right] \quad , \qquad (53)$$

where we used that $\psi = \rho_a/\rho_a^0$ is identical to the volume fraction of the asphaltene, while $A \approx 0.5$ and $b \approx 25.75$ are realistic values. Note that for the fully loaded interface (i.e. $\psi = 1$), the relative viscosity is $\approx 10^{10}$, i.e. even a thin (~ 1 nm), fully loaded interface might represent a solid wall for the water and the heptane. This is in a good agreement with experimental observations[42,43]. Therefore, it is reasonable to assume that the formation of these walls can block the hydrodynamics driven phase separation mechanism, thus stabilizing an emulsion on the hydrodynamic time scale.

The chosen physical parameters result in the model parameters $\tilde{\tau}_\psi = 0.073$, $\tilde{w} = 1.73 \times 10^4$, whereas the dimensionless viscosities read as $\tilde{\nu}_w = 2857$ and $\tilde{\nu}_h = 1633$ for the pure water and heptane, respectively. The effect of the asphaltene is taken into account as

$$\tilde{\nu}(\phi,\psi) = \left(\frac{1+\phi}{2}\right)\tilde{\nu}_w + \left(\frac{1-\phi}{2}\right)\tilde{\nu}_h + A\left[\exp(b\,\psi) - 1\right] \quad , \qquad (54)$$

where we use $A = 10^{-6}$, prescribing a viscosity contrast $\approx 10^2$ for the fully loaded interface ($\phi = 0$, $\psi = 1$) relative to the average liquid viscosity, $(\tilde{\nu}_w + \tilde{\nu}_h)/2$. Although this modification is necessary for numerical reasons[44], it results in a negligible variation of the bulk liquid viscosities even for $x = 20\%$ asphaltene content. Since the asphaltene is insoluble in the water[45], this is realistic in the water phase, while the real relative viscosity of the heptane prescribes a contrast of two orders of magnitude for $x = 20\%$. Nevertheless, in reality we use significantly less amount of the surfactant, i.e. $x \sim 1\%$, prescribing approximately 10% change in the viscosity of the bulk heptane. The $x = 20\%$ concentration is needed only because of the limited size of the numerical simulations, therefore, our choice $A = 10^{-6}$ mimics a realistic scenario well. We also mention, that scaling up the simulations together with proper handling of the solid-body like ranges necessitates the development of new numerical methods, which is out of the scope of the present study.

4.2.2 Competing time scales

In order to investigate the kinetics of phase separation, time-dependent simulations were performed by using Eqns. (29)-(32). We solved the equations in 2 dimensions on a square-shaped domain of size 4096×4096, with spatial time step $h = 0.5$, in the presence ($\tilde{w} = w_0$) and without ($\tilde{w} \equiv 0$) fluid flow. The time increments were $\Delta t = 0.005$ and $\Delta t = 0.1$, respectively. The computational domain was chosen to be periodic, therefore, an operator-splitting based, pseudo-spectral, semi-implicit numerical method was used to solve the equations[44]. In this case the incompressibility condition prescribed by Eq. (32) can be eliminated in the Chorin's projection method[46], resulting in significantly improved runtime. The initial condition of the simulations was chosen as follows: $\phi(\mathbf{r},0) = A\mathscr{R}[-1,1]$, where $\mathscr{R}[-1,1]$ is a uniformly distributed random number on $[-1,1]$ and $A \ll 1$, and $\psi(\mathbf{r},0) = \Psi$ (average surfactant load). Since this is a slightly perturbed unstable equilibrium state, the system is expected to undergo spinodal decomposition.

Similarly to our previous work, we measured the amount of

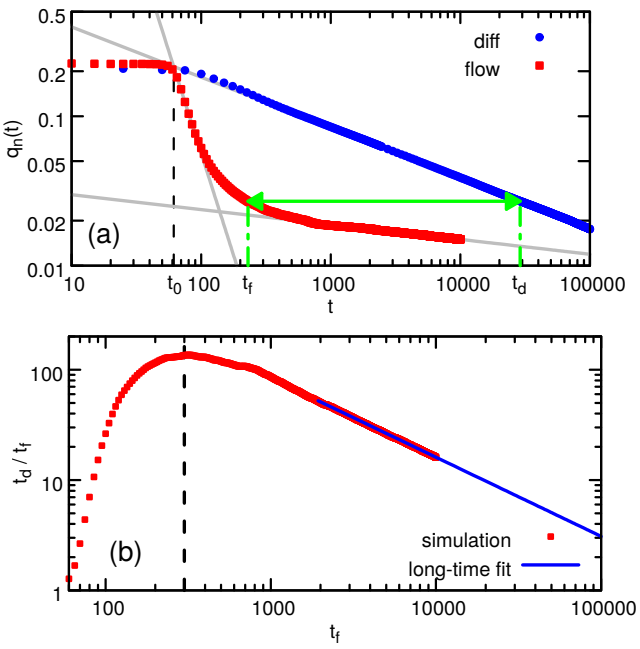

Fig. 5 Phase separation in the surfactant-free system. (a) Amount of interfaces as a function of time in case of pure diffusion dynamics (blue circles) and coupled hydrodynamics (red squares), respectively. (b) Relative time t_d/t_f as a function of t_f, indicating the speed of phase separation in the fluid-flow assisted system relative to the pure diffusion dynamics. The definitions of t_f and t_d are shown by panel a. For more details, see the text.

interfaces as a function of time:

$$q(t) := \frac{1}{V}\int dV \left\{ [\nabla(2\,\theta[\phi(\mathbf{r},t)]-1)]^2 \right\} \quad , \tag{55}$$

where $\theta(x)$ is the heaviside step function, therefore, $2\,\theta[\phi(\mathbf{r},t)]-1$ generates -1 where $\phi(\mathbf{r},t) \leq 0$, and $+1$ otherwise. This step is necessary because of the enormous spatial inhomogeneity and temporal variation of the liquid-liquid interface width, which is expected in case of the presence of the surfactant. With this simple projection, however, $q(t_1)$ and $q(t_2)$ (where $t_1 \neq t_2$) measured on the same simulation become comparable. In 2 dimensions, the discretization of Eq. (55) reads as:

$$q_n(t) := \left(\frac{h}{N}\right)^2 \sum_{i,j} \left[\left(\frac{\hat{\phi}^t_{i+1,j} - \hat{\phi}^t_{i-1,j}}{2h} \right)^2 + \left(\frac{\hat{\phi}^t_{i,j+1} - \hat{\phi}^t_{i,j-1}}{2h} \right)^2 \right] \quad , \tag{56}$$

where N is the linear size of the computational grid, and $\hat{\phi}^t_{i,j} = -1$ for $\phi^t_{i,j} \leq 0$ and $+1$ otherwise.

First, the time evolution of the surfactant-free system was investigated. The amount of interfaces as a function of time is shown by Fig. 5(a). At a certain time point t_0 (indicated in the figure), the system starts to separate in both cases. t_0 is called a "numerical incubation time", which can be related to the uncertainty of $q_n(t)$ emerging simply from the numerical discretization itself. After t_0, however, both modes show a simple power function behaviour $q_n(t) = (t/\gamma)^{-p}$, which applies for the

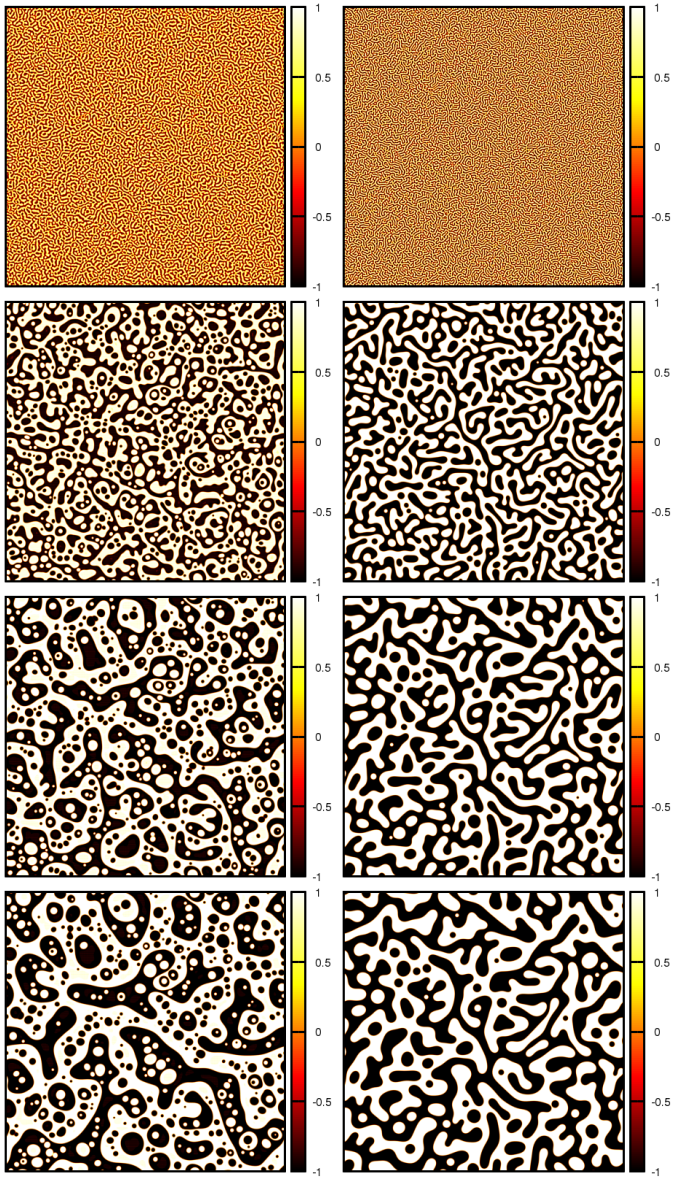

Fig. 6 Snapshots of the liquid-liquid order parameter (ϕ) from time dependent simulations in the surfactant-free system, taken at time points $t = 75, 125, 175$ and 225 (from top to bottom, respectively) in case of fluid-flow assisted kinetics (left column) and at $t = 174, 620, 17054$ and 26934 in case of simple diffusion dynamics (right column), respectively. The corresponding time points indicate the same amount of interfaces $q(t)$ defined by Eq. (55).

diffusion dynamics even for long times with $p_d = 0.34195$ and $\gamma_d = 0.7466$. In contrast, the fluid-flow assisted system features a transition from an early stage behaviour characterized by $p^e_f = 2.7$ and $\gamma^e_f = 34.727$ to a late stage mode yielding $p^l_f = 0.1$ and $\gamma^l_f = 4.7863 \times 10^{-15}$. In order to compare the speed of phase separation for the two modes, first we fix the amount of surfaces (q_0), then determine t_d and t_f from $q^d_n(t_d) = q^f_n(t_f) = q_0$ [as indicated by Fig. 5(a)], where $q^d_n(t)$ and $q^f_n(t)$ are the total amounts of interfaces in case of the diffusion and fluid-flow assisted kinetics, respectively. The result for t_d/t_f as a function of t_f are shown in Fig 5(b). For short times ($t \in [0, \approx 300]$), the fluid-flow

This journal is © The Royal Society of Chemistry [year]

assisted dynamics accelerates compared to the diffusion kinetics. The maximum of the curve indicates an enormous speed-up of the fluid-flow assisted dynamics, in the order of magnitude 10^2. This means that the diffusion dynamics needs roughly $100\times$ longer time to reach the same state [in terms of $q_n(t)$] that the fluid flow assisted kinetics reaches at $t = 300$. This is also illustrated in Fig 6. For larger times ($t \in [10^3, 10^4]$), however, the fluid-flow assisted dynamics decelerates significantly. The long-time fit it reveals that the time derivative of $q_n^f(t)$ is even smaller than that of $q_n^d(t)$. Since our scale of interest is basically the hydrodynamic scale, the phase separation practically stops. A possible explanation of this mode switching can be the following. First, the strongly non-equilibrium initial state of the matter generates so significant velocity field, that the hydrodynamic scale becomes dominant. The fluid is, however, viscous, meaning that without any internal (thermal) fluctuations and external forces (such as gravity or shearing), the flow will be suppressed. When this happens, the velocity field vanishes [$\mathbf{v}(\mathbf{r},t) \to 0$], therefore, the system switches back to the diffusion dynamics (long time behaviour).

Besides illustrating the contrast in the speed of phase separation between the diffusion and fluid flow coupled dynamic modes, Fig 6 also contains important informations regarding the forming patterns. Since the average volume fraction was chosen to be $\Phi := (1/V)\int dV\{\phi(\mathbf{r},t)\} = 0$, we have a transitional system. Indeed, it is impossible to judge from Fig 6 whether we have heptane in water or water in heptane in case of the diffusion dynamics, but the pattern is qualitatively different in case of the fluid-flow assisted kinetics. The reason is that in case of the diffusion dynamics we have a completely symmetric system at both levels, i.e. the level of the free energy and the dynamic equations. In contrast, with fluid flow coupling we introduce asymmetry in the viscosities, since the there is a viscosity contrast of roughly 2 between the bulk viscosities of the water and the heptane. This symmetry breaking leads to the formation of water-rich and heptane-rich areas, containing heptane and water bubbles, respectively.

As a next step, surfactant has been added to the system. The applied average amounts defined by

$$\Psi := \frac{1}{V}\int dV\{\psi(\mathbf{r},t)\} \tag{57}$$

were $\Psi = 0.05, 0.1, 0.15$ and 0.2, respectively. The results for $q_n(t)$ are summarized in Fig. 7, together with the results for the surfactant-free case. In order to isolate the effect attributed solely to the interfacial tension drop, the pure diffusion mode is investigated first. As shown by Fig. 8(a), $q_n(t)$ scales for short times as:

$$q_n(t) = [t/\tau(\Psi)]^{-q} \quad . \tag{58}$$

Using the fit $\log[q_n(t)] = -q\log(t) + p(\Psi)$ resuls in $\tau(\Psi) = \exp[p(\Psi)/q]$. Therefore, the dynamic factor defined as

$$s(\Psi) := \frac{\tau(0)}{\tau(\Psi)} = \exp\left[\frac{p(0)-p(\Psi)}{q}\right] \tag{59}$$

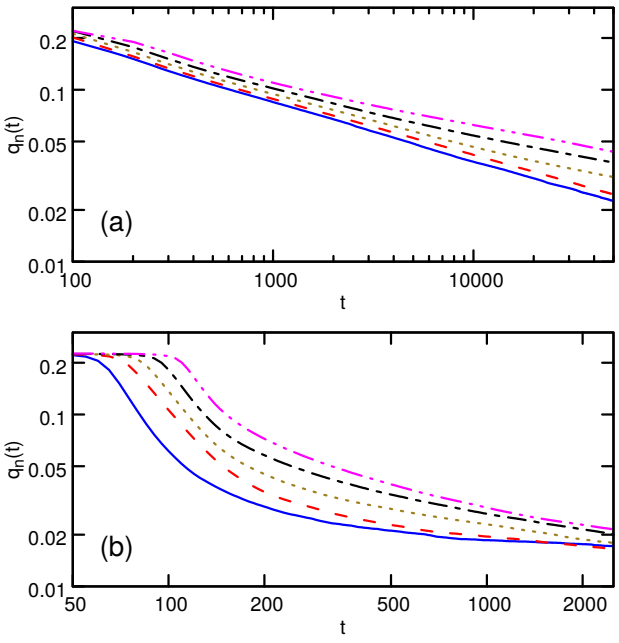

Fig. 7 Effect of adding surfactant to the system in case of (a) pure diffusion, and (b) fluid-flow coupled dynamics. The curves correspond to average surfactant load $\Psi = 0.0, 0.05, 0.1$ and 0.2 (from bottom to top on each panel), respectively.

expresses the speeddiof phase separation relative to the surfactant-free system[27]. The linear fit on the log-log plot resulted in $q = 0.3485$, and $p(\Psi) - p(0) = 0.0045564, 0.011473, 0.020232$ and 0.030772 for $\Psi = 0.05, 0.1, 0.15$ and 0.2, respectively. The corresponding dynamic factors are shown by the dots in Fig 8(b). For comparison, the dashed line shows the relative interfacial tension $\kappa(I) \approx 1 - 0.02I - 0.015276I^2$ for $I \to 0$ [see Fig 4(b)], where the total absorbed surfactant amount is calculated as $I = 9\Psi$. The excellent agreement in the characteristic behaviour of the dynamic factor and the relative interfacial tension shows that *in case of the diffusion dynamics the phase separation is driven by the interfacial tension drop*. This is also in agreement with our former results for systems featuring relatively low interface loads $[(\psi_a - \psi_0)/\psi_0 \ll 1]$[27]. Indeed, the small interfacial tension drop suggest small (average) total absorbed amount as well: For example, at $\Psi = 0.15$ the conversion between the total absorbed amount and the average surfactant concentration results in $I = 9\Psi = 1.35$. Assuming that the surfactant field can be approximated as $\psi(x) \approx \psi_0 + A\,\mathrm{sech}(x/2)^4$, the amplitude A and the total absorbed amount are related as $I = \int_{-\infty}^{+\infty} dx\{\psi(x) - \psi_0\} = (8/3)A$, resulting in $A = (3/8)I \approx 1/2$ for $\Psi = 0.15$. The estimated maximum of the surfactant field then reads as $\psi_a \approx \Psi + A = 0.65$, which is also in agreement with the simulation results (see Fig. 9).

Finally, the early stage behaviour of the fluid-flow assisted kinetics has been addressed. As indicated by Fig 10(a), the scaling behaviour $q_n(t) = (t/tau)^{-q}$ also applies here, however, the emerging dynamic factors show a different behaviour compared to the diffusion case, as shown in Fig 10(b). First, the reduction in the

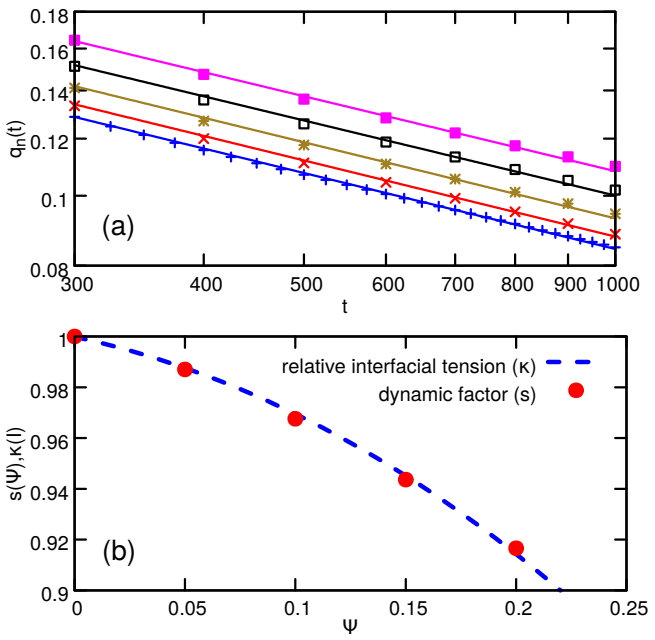

Fig. 8 Early stage of the time evolution of the diffusion system for different average surfactant loads. (a) Amount of interfaces $q_n(t)$ as a function of time in case of $\Psi = 0.0, 0.05, 0.10, 0.15$ and 0.2 (from bottom to top), respectively. (b) Dynamic factor and relative interfacial tension as a function of the average surfactant load Ψ.

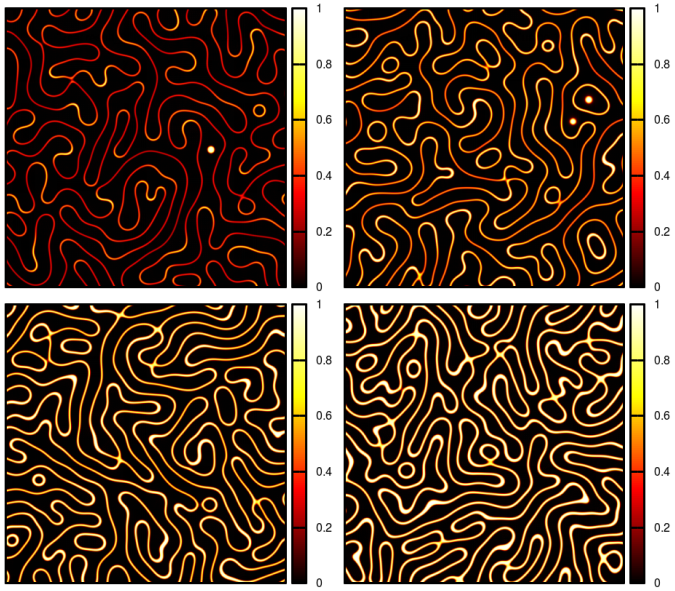

Fig. 9 Surfactant concentration at $t = 500$ in case of pure diffusion dynamics, for average surfactant loads $\Psi = 0.05$ (top-left), 0.10 (top right),0.15 (bottom left) and 0.2 (bottom right). The measured dynamic factors indicate the (average) total absorbed amounts $I = 0.45, 0.9, 1.35$ and 1.8, while the corresponding average interface loads read as $\psi_a \approx 0.22, 0.44, 0.66$ and 0.88, respectively. For better visibility, only a 256×256 pixel part of the 4096×4096 simulation domain is shown.

speed is much larger compared to the diffusion mode ($\kappa = 0.55$ vs $\kappa = 0.92$ at $\Psi = 0.2$, for example). Second, the tendency is perfectly linear in the range $\Psi \in [0.05, 0.2]$, which is not true for $\kappa(I)$. Nevertheless, the average total absorbed amount I can be estimated as a function of Ψ as follows. The volumetric integral of the absorbed surfactant reads as $\Sigma = \int dV\{\psi(\mathbf{r},t) - \psi_0(t)\}$, where $\psi_0(t)$ is the actual background. The average total absorbed amount can be defined via $\Sigma = \bar{I}\Gamma$, where Γ is the total length of the interfaces, and $\bar{I}$ is the average total amount of surfactant absorbed by the interfaces. On the other hand, $\int dV\{\psi(\mathbf{r},t)\} = (Nh)^2\Psi$. If Γ and ψ_0 are measurable, the average total absorbed amount can be expressed as $\bar{I} = (Nh)^2[\Psi - \psi_0(t)]/\Gamma$. Γ is measured from the simulations as follows:

$$\Gamma := h \sum_{i,j} \alpha_{i,j} \quad , \tag{60}$$

where $\alpha_{i,j}$ is equal to 1, if $\phi_{i,j}\phi_{i+1,j} < 0$ and $\phi_{i,j}\phi_{i,j+1} > 0$ [the interface normal is (1,0)], or $\phi_{i,j}\phi_{i+1,j} > 0$ and $\phi_{i,j}\phi_{i,j+1} < 0$ [the interface normal is (0,1)], $\sqrt{2}$ if $\phi_{i,j}\phi_{i+1,j} < 0$ and $\phi_{i,j}\phi_{i,j+1} < 0$ [the interface normal is (1,1)], and 0 otherwise (no interface). In addition ψ_0 is calculated as

$$\psi_0 = \frac{\sum_{i,j} \beta_{i,j}\, \psi_{i,j}}{\sum_{i,j} \beta_{i,j}} \quad , \tag{61}$$

where $\beta_{i,j} = 1$ if $|\phi_{i,j}| > 0.8$ (i.e. ϕ is outside of the $10\% - 90\%$ interface width), and 0 otherwise. With these definitions, the corresponding average total absorbed amounts were found to be $\bar{I} = 0.8375, 1.3975, 1.6811$, and 1.6876, respectively, while the corresponding relative interfacial tensions are shown in Fig 10(b). The estimated interfacial tension drop $\kappa(\bar{I})$ shows the same tendency as in the case of the pure diffusion dynamics (at $\Psi = 0.2$, $\kappa = 0.92$ in both cases, for example), which is not that surprising, taking into account that (i) we use the same amounts of surfactant, and (ii) no thick interfaces are present in the system yet (see Fig. 11). This analysis indicates that there is an extra effect on the speed of phase separation, which is $4-5\times$ stronger compared to the effect of the interfacial tension drop. Since this effect is proportional to the surfactant load, it clearly originates from the surfactant viscosity: According to Eq. (54), it is 2 orders of magnitude higher in the bulk surfactant than in the liquid, i.e. loaded interfaces suppress the fluid flow proportional to $\bar{I} \propto \Psi$. In the later stage of the process, as discussed before, the flow becomes totally sedated, drawing the system back to the diffusion time scale, thus leading to the formation of a 'dynamically stabilized' emulsion (see Fig 12). The term 'dynamically stabilized' means that the emulsion forms on the hydrodynamic time scale, then develops on the diffusion times scale.

4.3 Limitations of the dynamic equations

Although the parameters of the theory have been fitted to MD results on an acceptable level, Fig. 3(d) shows the limitation of the theory implicitly. The liquid-liquid equilibrium profile, $\phi^*(x)$ does not recover $\rho_w(x)/\rho_w^0 - \rho_h(x)/\rho_h^0$ perfectly. Nevertheless, profiles similar to the MD results can be achieved via

$$\frac{\rho_w(x)}{\rho_w^0} - \frac{\rho_h(x)}{\rho_h^0} = [1 - \psi^*(x)]\phi^*(x) \tag{62}$$

This journal is © The Royal Society of Chemistry [year]

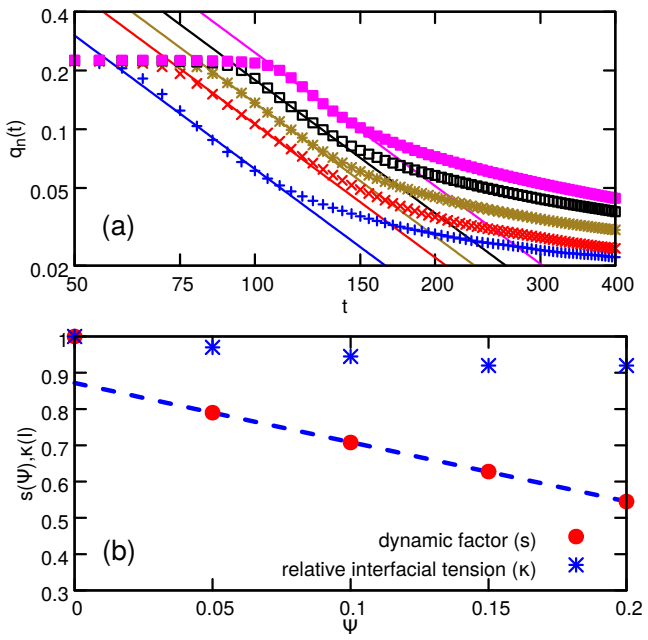

Fig. 10 Early stage of the time evolution of the fluid-flow assisted system for different average surfactant loads. (a) Amount of interfaces $q_n(t)$ as a function of time in case of $\Psi = 0.0, 0.05, 0.10, 0.15$ and 0.2 (from bottom to top), respectively. (b) Dynamic factor and relative interfacial tension as a function of the average surfactant load Ψ.

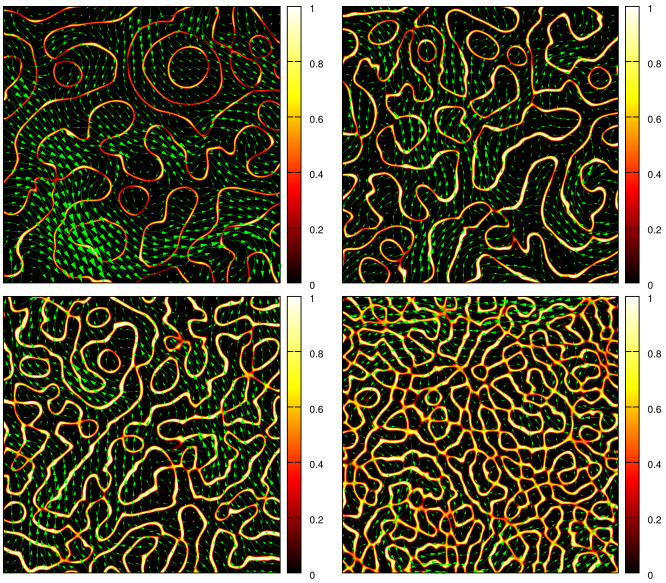

Fig. 11 Surfactant concentration at $t = 125$ (early stage) in case of fluid-flow coupled kinetics, for $\Psi = 0.05, 0.10$ (upper row, from left to right), and $0.15, 0.2$ (lower row, from left to right), respectively. The flow field is indicated by the green arrows. for better visibility only a 256×256 part of the simulation area is shown.

applies instead of Eq. (49), indicating another possible interpretation of ϕ:

$$\phi^*(x) = \frac{n_w(x) - n_h(x)}{1 - n_a(x)} \quad , \tag{63}$$

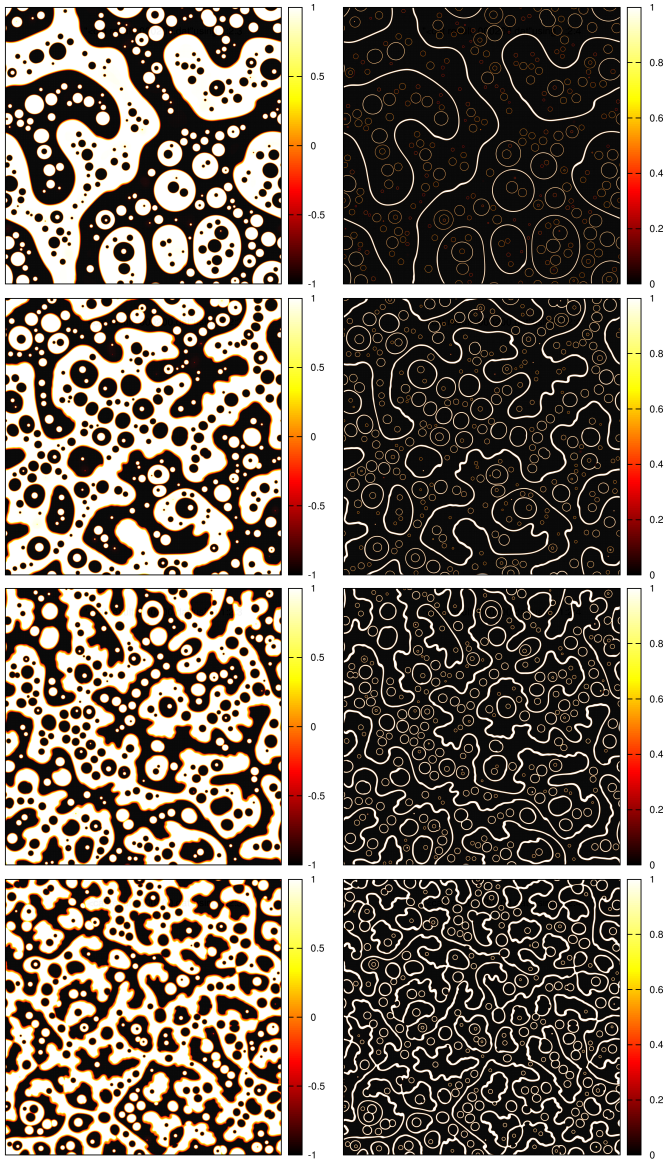

Fig. 12 Liquid-liquid order parameter (on the left) and corresponding surfactant concentration (on the right) at $t = 1000$ (late stage) in case of fluid-flow coupled kinetics, for $\Psi = 0.05, 0.10, 0.15$ and 0.2 (from top to bottom), respectively.

where $n_i(x) = \rho_i(x)/\rho_i^0$ is the normalized mass (or number) density of specie $i = w, h, a$. Although Eq. (62) represent a consistent interpretation, it clearly shows, that ϕ becomes non-conserved. Although it has no effect on equilibrium properties, as long as $(\delta\tilde{F}/\delta\phi)|_{\phi_0,\psi_0} = 0$ applies, the dynamic equation for ϕ must be modified accordingly. Assuming conservative dynamics for n_w and n_h, and considering the transformation $F(\phi,\psi) = F[(n_w - n_h)/(1 - n_a), n_a]$ yields

$$\begin{aligned} \dot{\phi} &= \frac{(\dot{n}_w - \dot{n}_h) + \dot{\psi}\phi}{1-\psi} \\ &= \frac{\nabla\left[\tilde{M}(\phi,\psi)\nabla\left(\frac{\delta F}{\delta\phi}\frac{1}{1-\psi}\right)\right] + \frac{\phi}{\tilde{\tau}}\nabla\left[\psi(1-\psi)\nabla\frac{\delta F}{\delta\psi}\right]}{1-\psi} \quad , \end{aligned} \tag{64}$$

where $\tilde{M}(\phi,\psi)$ is a general mobility function and we applied the chain rule $\frac{\delta F}{\delta n_i} = \frac{\delta F}{\delta \phi}\frac{\partial \phi}{\partial n_i} + \frac{\delta F}{\delta \psi}\frac{\partial \psi}{\partial n_i}$ for the functional derivative. Note, that $\delta F/\delta\phi = 0$ and $\delta F/\delta\psi = \mu$ transforms into $\frac{\delta F}{\delta n_a} = \mu$ and $\frac{\delta F}{\delta n_w} = \frac{\delta F}{\delta n_h} = 0$, i.e. equilibrium transforms into equilibrium. Without going further, Eq. (64) is clearly divergent for $\psi \to 1$, i.e. for large interface loads. It is not that surprising, taking into account that the densities n_w and n_h are equal for $\phi = 0$ *or* $\psi = 1$. The latter is a "dangerous" solution, expressing that $\psi = 1$ always represents the same physical state, regardless the value of ϕ, and we should not forget, that the derivation of the dynamic equation described by Eq. (64) is based on the dynamic behaviour of the physical variables. This is a clear limitation of the model, thus necessitating a full treatment of the problem with the 3 (independent) densities.

5 Conclusions

In this work we applied a Ginzburg-Landau theory of surfactant assisted liquid phase separation to model the dynamic emulsion formation in the heptane/water/asphaltene system, which has a high industrial importance in crude oil recovery. As a continuation of our previous work, we analysed the equilibrium properties of the model in case of high interface loads and negligible bulk loads. From the viewpoint of the dynamic behaviour of the system, both diffusion and hydrodynamic effects were considered. The major findings of the research are the followings: (i) The Ginzburg-Landau theory of surfactant assisted liquid phase separation describes highly loaded liquid-liquid interfaces quantitatively, recovering the equilibrium interface profiles and the surfactant concentration dependence of the relative interfacial tension. Fitting the model parameters to the results of molecular dynamics simulations (equilibrium profiles) yielded a relative interfacial tension saturating for high surfactant concentrations (total absorbed amount of surfactant), a tendency can also be observed in real crude oil / water / asphaltene samples. This finding directly verifies the mathematical concept of the surfactant coupling in the free energy functional, which otherwise was set up heuristically. (ii) The fluid flow has a significant effect of the behaviour of the system, yielding faster phase separation process than it is predicted by a simple diffusion dynamics. Far from equilibrium, the non-classical Korteweg stress generates significant velocity field which then dominates the early stage of the phase separation process. The fluid-flow assisted phase separation can be then even $100\times$ faster than the diffusion driven, but due to the viscosity the fluid flow tails away and the system enters a (mostly) diffusion-driven late stage mode. This picture can be refined by applying internal fluctuations and external forces, which is a topic of future research. The main finding is that the fluid flow is not negligible even on the mesoscale. (iii) In addition to the interfacial tension drop, a much larger effect can be observed in the slowdown of the phase separation as a function of the surfactant load. It is attributed to the surfactant concentration dependence of the viscosity: Since the bulk surfactant areas behave as solid for the fluid flow, the forming surfactant 'walls' sedate the fluid flow (proportional to the amount of the added surfactant), thus leading to the formation of a dynamic emulsion via terminating drop coalescence on the hydrodynamic time scale, which is a topic a future research.

Finally we address the physical size and time scale of the calculations. Taking into account that the surfactant-free interface is atomic (so $\delta_0 \sim nm$) results in the physical size of the simulation are in the order of μm^2, while $D_0 \sim 10^9 m^2/s$ results in the time scale $\tau \sim ns$. The early stage of the fluid flow assisted process happens in a few $0.1\mu s$ ($t = 10^2$), while the late stage is valid on the $10\mu s$ scale ($t = 10^4$) and above. These data show the robustness of the model: using data from the nanoscale (MD) it predicts the behaviour of the system on the mesoscale.

We also have to emphasize, that this work also has interdisciplinary significance. The theory is general, therefore, it can be applied for various real systems, including surfactant coated free surfaces of liquids appearing in medical sciences[47]. The present Ginzburg-Landau theory, however, has some limitations. The usual interpretation of the variables as (normalized) density difference (ϕ) and surfactant mole fraction (ψ) is not sufficient, taking into account that the emerging equilibrium profiles show rather qualitative agreement with the results of molecular dynamics simulations close to the center of the interface, in case of high surfactant loads. In contrast, suitable transformation of ϕ and ψ can be found to recover the normalized equilibrium density profiles of the species. Nevertheless, this transformation yields a non-conserved ϕ, and prescribes a special kinetic equation. Unfortunately, the singular transformation from the densities to ϕ and ψ yield singular equation of motion as well, necessitating the usage of the normalized physical densities as order parameters in the model.

Acknowledgement

The authors thank Yunfeng Liang from Kyoto University, Japan. This work has been supported by the VISTA basic research programme project No. 6359 "Surfactants for water/CO_2/hydrocarbon emulsions for combined CO_2 storage and utilization" of the Norwegian Academy of Science and Letters and the Statoil.

References

1 J. Sjøblom, *Emulsions and Emulsion Stability: Surfactant Science Series/61*, Taylor & Francis, 1996.

2 D. Sarker, *Pharmaceutical Emulsions: A Drug Developer's Toolbag*, Wiley, 2013.

3 D. Myers, *Surfactant Science and Technology*, Wiley, 2005.

4 D. Halpern, O. E. Jensen and J. B. Grotberg, *J. Appl. Physiol.*, 1998, **85**, 333–352.

5 B. A. Hills, *J. Appl. Physiol.*, 1999, **87**, 1567–1583.

6 G. Ahearn, *J. Am. Oil Chem. Soc.*, 1969, **46**, 540A–580A.

7 S. Iglauer, Y. Wu, P. Shuler, Y. Tang and W. A. G. III, *J. Petrol. Sci. Eng.*, 2010, **71**, 23 – 29.

This journal is © The Royal Society of Chemistry [year]

8 S. Q. Tunio, A. H. Tunio, N. A. Ghirano and Z. M. El Adawy, *Intl. J. Appl. Sci. Tech.*, 2011, **1**, 143–153.

9 Z. Song, Z. Li, M. Wei, F. Lai and B. Bai, *Computers & Fluids*, 2014, **99**, 93 – 103.

10 S. S. Adkins, X. Chen, I. Chan, E. Torino, Q. P. Nguyen, A. W. Sanders and K. P. Johnston, *Langmuir*, 2010, **26**, 5335–5348.

11 B. Bharatwaj, L. Wu and S. R. P. da Rocha, *Langmuir*, 2007, **23**, 12071–12078.

12 Y. Liang, 2015, personal communication.

13 V. Pauchard, J. P. Rane, S. Zarkar, A. Couzis and S. Banerjee, *Langmuir*, 2014, **30**, 8381–8390.

14 Y. Mikami, Y. Liang, T. Matsuoka and E. S. Boek, *Energy & Fuels*, 2013, **27**, 1838–1845.

15 M. Sedghi, L. Goual, W. Welch and J. Kubelka, *J. Chem. Phys. B*, 2013, **117**, 5765–5776.

16 J. P. Rane, D. Harbottle, V. Pauchard, A. Couzis and S. Banerjee, *Langmuir*, 2012, **28**, 9986–9995.

17 G. Gompper and S. Zschocke, *Phys. Rev. A*, 1992, **46**, 4836–4851.

18 O. Theissen and G. Gompper, *Eur. Phys. J. B*, 1999, **11**, 91–100.

19 T. Teramoto and F. Yonezawa, *J. Colloid Interf. Sci.*, 2001, **235**, 329 – 333.

20 R. van der Sman and S. van der Graaf, *Rheol. Acta*, 2006, **46**, 3–11.

21 H. Diamant and D. Andelman, *Europhys. Lett.*, 1996, **34**, 575–580.

22 C.-H. Teng, I.-L. Chern and M.-C. Lai, *Discrete Cont. Dyn. B*, 2012, **17**, 1289 – 1307.

23 H. Liu and Y. Zhang, *J. Comp. Phys.*, 2010, **229**, 9166 – 9187.

24 Li, Y. and Kim, J., *Eur. Phys. J. B*, 2012, **85**, 340.

25 A. Yun, Y. Li and J. Kim, *Appl. Math. Comput.*, 2014, **229**, 422 – 432.

26 S. Engblom, M. Do-Quang, G. Amberg and A.-K. Tornberg, *Commun. Comput. Phys.*, 2013, **14**, 879 – 915.

27 G. I. Tóth and B. Kvamme, *Phys. Rev. E*, 2015, **91**, 032404.

28 D. J. Korteweg, *Arch. Neerl. Sci. Ex. Nat.*, 1901, **6**, 1–24.

29 R. Evans, *Adv. Phys.*, 1979, **28**, 143–200.

30 R. Salmon, *Annu. Rev. Fluid Mech.*, 1988, **20**, 225–256.

31 A. A. Wheeler and G. B. McFadden, *Proceedings of the Royal Society of London. Series A: Mathematical, Physical and Engineering Sciences*, 1997, **453**, 1611–1630.

32 D. M. Anderson, G. B. McFadden and A. A. Wheeler, *Annu. Rev. Fluid Mech.*, 1998, **30**, 139–165.

33 D. Anderson, G. McFadden and A. Wheeler, *Physica D*, 2000, **135**, 175 – 194.

34 M. Conti, *Phys. Rev. E*, 2001, **64**, 051601.

35 M. Conti and M. Fermani, *Phys. Rev. E*, 2003, **67**, 026117.

36 J. Kim and J. Lowengrub, *Intf. Free Bound.*, 2005, **7**, 435 – 466.

37 G. Alvarez, S. Poteau, J.-F. Argillier, D. Langevin and J.-L. Salager, *Energy & Fuels*, 2009, **23**, 294–299.

38 M. Ghanavati, M.-J. Shojaei and A. R. S. A., *Energy & Fuels*, 2013, **27**, 7217–7232.

39 W. S. Price and O. Söderman, *J. Phys. Chem. A*, 2000, **104**, 5892–5894.

40 S. Wang, J. Xu and H. Wen, *Comp. Phys. Commun.*, 2014, **185**, 3069 – 3078.

41 P. Först, F. Werner and A. Delgado, *Rheol. Acta*, 2000, **39**, 566–573.

42 P. Bouriat, N. El Kerri, A. Graciaa and J. Lachaise, *Langmuir*, 2004, **20**, 7459–7464.

43 V. Pauchard, J. SjÃűblom, S. Kokal, P. Bouriat, C. Dicharry, H. MÃijller and A. al Hajji, *Energy & Fuels*, 2009, **23**, 1269–1279.

44 G. Tegze, G. Bansel, G. I. Tóth, T. Pusztai, Z. Fan and L. Gránásy, *J. Comp. Phys.*, 2009, **228**, 1612 – 1623.

45 G. Yu, K. Karinshak, J. H. Harwell, B. P. Grady, A. Woodside and M. Ghosh, *Colloid. Surface. A*, 2014, **441**, 378 – 388.

46 E. R. Peyret and R. G. de Vahl Davis, *Appl. Mech. Rev.*, 2003, **56**, B13–B15.

47 S. L. Strickland, M. Hin, M. R. Sayanagi, C. Gaebler, K. E. Daniels and R. Levy, *Phys. Fluids*, 2014, **26**, 042109.